Kinetic Modeling of the Dynamic PET Brain Data Using Blind Source Separation Methods

Ondřej Tichý[a,b], Václav Šmídl[a]

[a]Department of Adaptive Systems,
Institute of Information Theory and Automation,
Prague, Czech republic

[b]Department of Mathematics,
Faculty of Nuclear Sciences and Physical Engeneering,
Prague, Czech republic

***Abstract*—Image-based definition of regions of interest is a typical prerequisite step for estimation of time-activity curves in dynamic positron emission tomography (PET). This procedure is done manually by a human operator and therefore suffers from subjective errors. Another such problem is to estimate the input function. It can be measured from arterial blood or it can be searched for a vascular structure on the images which is hard to be done, unreliable, and often impossible. In this study, we focus on blind source separation methods with no needs of manual interaction. Recently, we developed sparse blind source separation and deconvolution (S-BSS-vecDC) method for separation of original sources from dynamic medical data based on probability modeling and Variational Bayes approximation methodology. We apply the methods on dynamic brain PET data and application and comparison of our S-BSS-vecDC algorithm with those of similar assumptions are given. The S-BSS-vecDC algorithm is publicly available for download.**

***Index Terms*—Blind Source Separation, Dynamic PET, Input Function, Deconvolution**

I. Introduction

Physical examination using scintigraphy [4] or positron emission tomography (PET) [8] allows us to see processes inside the living body without surgery. Contrast medium can be applied into the body and its spatial distribution can be measured for the selected part of body. In PET, the measured activity in each voxel is a superposition of the signal tissues. Since the measurement is done repetitively, a time distribution of the scanned region of body can be obtained. The task of medical analysis is to obtain the clear activity of each tissue separately.

In practice, the analysis of dynamic PET is often based on input function (IF), i.e. blood curve, knowledge [14]. This can be achieved using arterial blood sampling [7] which is very invasive and sensitive to errors. A number of methods has been proposed to lower invasiveness of measurement [3] or derive the IF directly from the dynamic PET images. In some cases, blood structure can be directly observed on the images. In this cases, a region of interest (ROI) can be manually placed on vascular structures and its related time-activity curve (TAC) can be obtained [6]. Manual selection of the ROIs may suffer from subjectivity. This issues has been addressed using automatic clustering methods [12].

This work was supported by the Czech Science Foundation, grant No. 13-29225S, and by the Grant Agency of the Czech Technical University in Prague, grant No. SGS14/205/OHK4/3T/14.

However, more important problem is that the selected blood structure typically accumulate activity not only from the blood but also from other tissues; hence, a mixture of TACs is obtained instead of the pure IF. Moreover, such a structure is often not present on scanned images and no such ROI with pure IF can be placed. Separation of mixed signals in general is the task for blind source separation (BSS) methods. They offer an automatic way for separation of tissues from the measured sequence. Some methods are general with no extra medical assumptions [13], [2] and provide non-negative matrix factorization essentially [11], [5]. Medically motivated extensions have been proposed based on compartmental modeling [15], [19] where detailed model of the tracer behavior is incorporated into the separation procedure. In our previous publication [17], we tried to offer a reasonable compromise between a domain specific BSS method and a medically focused BSS method.

Recently, we have studied the influence of the sparsity assumption on BSS problems, which means to reflect that the activity of each source is present only on limited region of recorded images [9]. We developed sparsity in blind source separation and deconvolution (S-BSS-vecDC) method [18] which assumes each TAC to be the results of a convolution between common input function and source-specific convolution kernel and source-images to be sparse. The sparsity is not strict but favored by proposed probabilistic model using automatic relevance determination principle [1].

The aim of this work is to compare existing methodology for tissue separation on data with easy-to-find TAC of the blood. We analyze data from dynamic PET of brain where structures with arterial blood are obvious and thus this data can be used as the simplest possible benchmark of separation methods. The comparison is given using both, slice by slice processing and the whole volume processing. It allows us to study the separation performance as well as the stability of algorithms.

II. Blind Source Separation Methods

The general assumptions of the blind source separation methods, which is common for all methods to be compared, will be summarized. Then, we will make detailed views on the selected methods.

The observed data are assumed to arise as a superposition of signals from underlying tissues and the signal is assumed

978-1-4799-5838-2/14/$31.00 @2014 IEEE

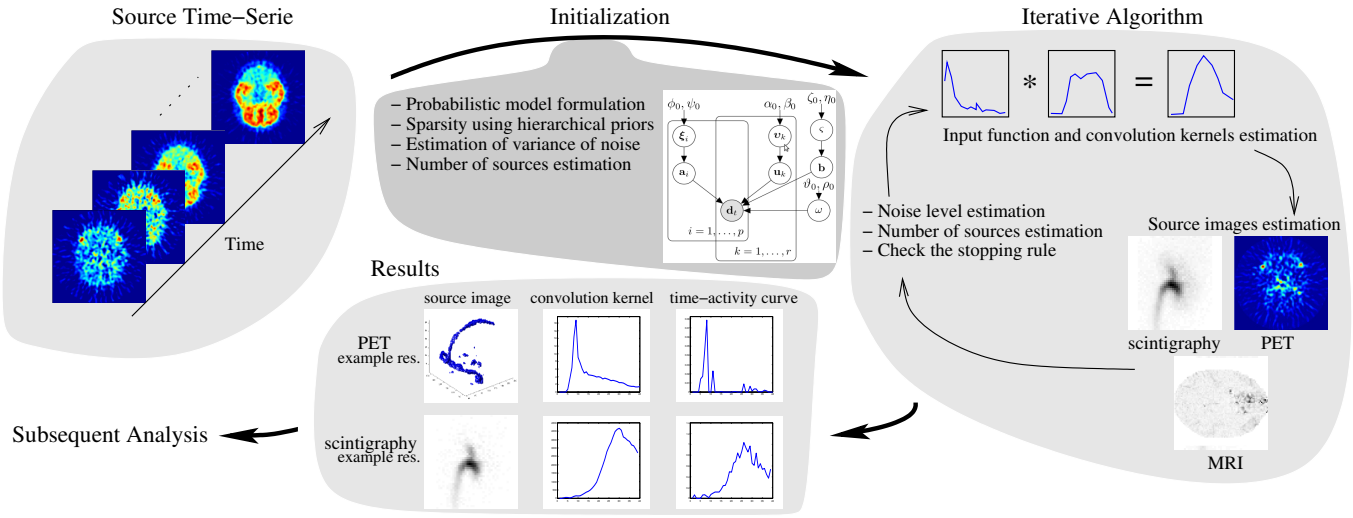

Figure 1. The S-BSS-vecDC method's flowchart.

to be degraded by a noise. The data at each time t is stored columnwise in vector $\mathbf{d}_t$. Since the number of voxels is p, $\mathbf{d}_t \in \mathbf{R}^{p\times 1}$. The vector $\mathbf{d}_t$ is assumed to be an observation of a superposition of r tissue images stored in vectors $\mathbf{a}_k \in \mathbf{R}^{p\times 1}, k = 1,\ldots,r$. Each tissue image is weighted by its related TAC $\mathbf{x}_k \in \mathbf{R}^{n\times 1}, k = 1\ldots,r$, where n is the number of measurements, $t = 1,\ldots,n$. Summarizing the vectors into matrices $D = [\mathbf{d}_1,\ldots,\mathbf{d}_n] \in \mathbf{R}^{p\times n}$, $A = [\mathbf{a}_1,\ldots,\mathbf{a}_r] \in \mathbf{R}^{p\times r}$, and $X = [\mathbf{x}_1,\ldots,\mathbf{x}_r] \in \mathbf{R}^{n\times r}$, the matrix formulation of the superposition problem can be written as

$$D = AX^T + E. \tag{1}$$

Here $()^T$ denotes transpose of a matrix or vector and E is the noise matrix of the same size as the data matrix D.

A. Blind Source Separation with Positivity

Additional biologically-motivated assumptions are imposed on the elements of (1) in the probabilistic model of Blind Source Separation with Positivity (BSS+): (i) all elements of the observed vectors $\mathbf{d}_t$ are positive, (ii) all elements of the tissue images $\mathbf{a}_k$ and the TACs $\mathbf{x}_k$ are also positive, and (iii) the number of relevant sources, r, is unknown. These assumptions are translated into probabilistic model as described in [13]. Moreover, the variance of noise is estimated as well as the relevant number of vectors, r, using automatic relevance determination (ARD) mechanism [1].

B. Factor Analysis with Integrated Regions of Interests

The Factor Analysis with Integrated Regions of Interests (FAROI) method [16] has the same advantage as BSS+ method; however, tissue images are modeled in more details. Each element of matrix A, $a_{i,k}$, has indicator $\mathbf{i}_{i,k}$ such as

$$\mathbf{i}_{i,k} = \begin{cases} 1 & \text{i-th pixel belongs to the k-th tissue} \\ 0 & \text{i-th pixel not belongs to the k-th tissue} \end{cases} \tag{2}$$

and then, the model for each pixel switched using this indicator as

$$f(a_{i,j}) = \begin{cases} \mathcal{U}(0,1) & \mathbf{i}_{i,j} = 1, \\ t\mathcal{N}(0,\xi_j^{-1}) & \mathbf{i}_{i,j} = 0, \end{cases} \tag{3}$$

where uniform distribution $\mathcal{U}(0,1)$ is a noisy part of tissue and truncated normal distribution $t\mathcal{N}(0,\xi_j^{-1})$, defined in Appendix A, is an informative part of tissue with unknown variance.

As a result, the FAROI model is capable to separate tissue images with small number of pixels which could be rejected as insignificant by the BSS+ model.

C. Blind Compartment Model Separation

The Blind Compartment Model Separation (BCMS) model [19] reflects that the TACs can be described by compartment model, where each TAC arise as a convolution between a common input function and a tissue-specific kernel [15]. Hence, each element of the matrix X, $x_{j,k}$, is modeled as a convolution between the input function, vector $\mathbf{b}$, and the convolution kernel $\mathbf{u}_k$ such as

$$x_{j,k} = \sum_{t=1}^{j} b_{j-t+1} u_{t,k}, \tag{4}$$

where the input function $\mathbf{b}$ is assured to be decreasing and kernels $\mathbf{u}_k$ are assured to be decreasing and piece-wise linear with constant plateau in the beginning and the decreasing to zero [10]. The limitation of BCMS method is its restrictive shape which is suitable only in limited number of situation.

D. Non-negative Matrix Factorization

Non-negative matrix factorization (NMF) [2] assumes that the data matrix $D \in \mathbf{R}^{p\times n}$ can be approximated by linear combination $D \approx AX^T$, where $A \in \mathbf{R}_+^{p\times r}$, and $X \in \mathbf{R}_+^{n\times r}$ is TACs recovering the columns of D using the columns of A. The number of sources, r, has to be given.

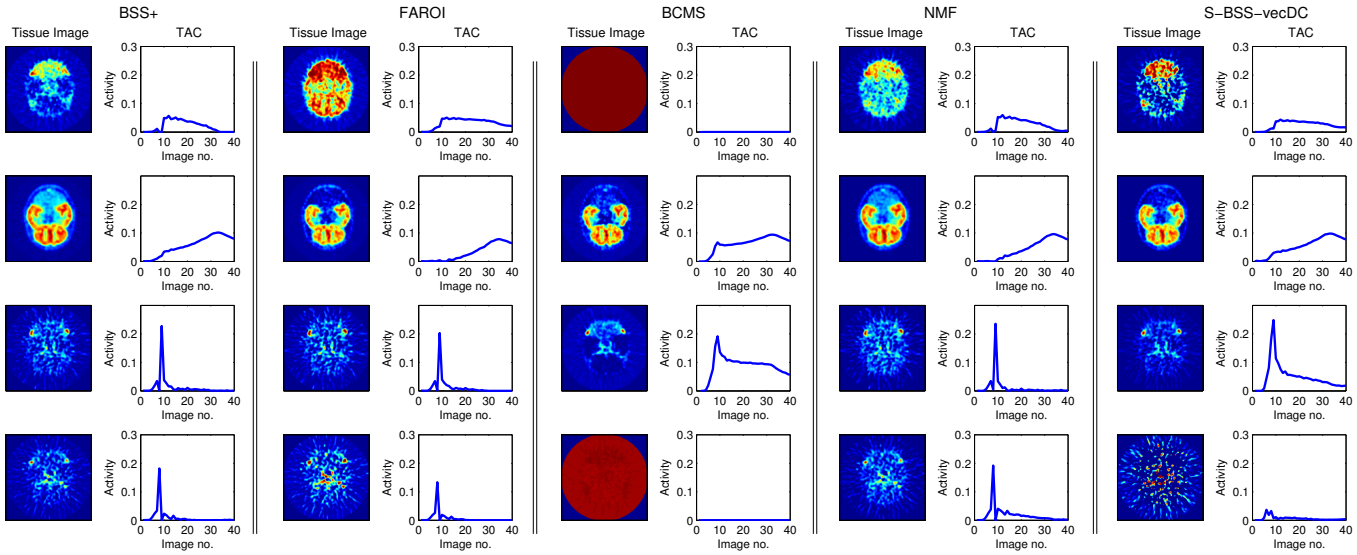

Figure 2. The example results from the BSS+, FAROI, BCMS, NMF, and S-BSS-vecDC algorithms are shown using sequence from the 10th slice. The estimated tissue images are in the left column and the estimated TACs are in the right column.

E. Sparsity in Blind Source Separation and Deconvolution

Sparse Blind Source Separation and Deconvolution (S-BSS-vecDC) method [18] applies the automatic relevance determination (ARD) mechanism [1] to more variables of the model. The convolution model of TACs (4) is also adopted; however, in more relaxed form than in the BCMS method. The convolutions kernels are not restricted to be in piece-wise linear form, the only imposed assumption is their sparsity, via the ARD methodology:

$$f(u_{j,k}|v_{j,k}) = t\mathcal{N}(0, v_{j,k}^{-1}, [0;\infty]),\ \forall j = 1,\dots,n, \quad (5)$$

$$f(v_{j,k}) = \mathcal{G}(\alpha_0, \beta_0). \quad (6)$$

Hence, each element of the convolution kernel is truncated to positive value, see Appendix A, and its variance $v_{j,k}$ is modeled as a Gamma prior and estimated jointly with the convolution kernel.

The sparsity prior is also used for each element $a_{i,k}$ of tissue images, matrix A, as

$$f(a_{i,k}|\xi_{i,k}) = t\mathcal{N}(0, \xi_{i,k}^{-1}, [0;1]),\ \forall i = 1,\dots,p, \quad (7)$$

$$f(\xi_{i,k}) = \mathcal{G}(\phi_0, \psi_0). \quad (8)$$

Note that in this case, the normal distribution (7) is truncated to real numbers from the interval $[0;1]$ which serves to better stability of solution.

The flowchart of the S-BSS-vecDC method is in Figure 1.

The algorithm implemented in MATLAB can be downloaded from http://www.utia.cas.cz/AS/softwaretools/image_sequences.

III. Experiments

We will demonstrate the separation ability of the compared algorithms on a real brain data from dynamic PET [12].

In this study, ^{18}F-altanserin was applied to a patient and scanned with an 18-ring GE-Advance scanner (General Electric Medical System, Milwaukee, WI, USA) which is able to record 3D scans. Each scan consists of 35 image slices with an interslice distance 4.25 mm. The data were reconstructed into a sequence of $128 \times 128 \times 35$ voxel matrices, $2 \times 2 \times 4.25$ mm each voxel, using software provided by the manufacturer. The sequence consists of 40 voxel matrices, $n = 40$. For illustration of the method, we selected the 10th slice; however all algorithms can proceed the full volume.

Separation of the tissue images on the 10th slide using BSS+, FAROI, BCMS, NMF, and S-BSS-vecDC algorithms are displayed in Figure 2 with $r = 4$. Note that the tissues separated by the S-BSS-vecDC algorithm have better anatomical meaning than those from the competing methods. The first tissue is clearly separated by the S-BSS-vecDC algorithm while there is a residual activity from arterial veins by the BSS+ and the FAROI algorithms and from both, arterial veins and the second tissue, by the NMF algorithm. The BCMS algorithm was not able to separate the first tissue. The third tissue, arterial veins, is again clearly separated by the S-BSS-vecDC algorithm while the BSS+, the FAROI, and the NMF algorithms split the arterial veins into two tissues mixed with the artifacts of the PET reconstruction. The BCMS algorithm combines the first tissue into the third tissue which can be recognized from its TAC. Moreover, the S-BSS-vecDC algorithm clearly separated the PET reconstruction artifacts as the forth estimate; hence, the previous three physiological tissues are cleared from these artifacts.

Demonstration of the better separation is given using blood tissue where manual TAC can be easily obtain. First, we placed the ROI of the arterial veins on the tested sequence, see Figure 3. Second, comparison of the manual obtained blood TAC with those obtained using automatic method (Figure 2, the third row) is given in Figure 4. It can be observed that the S-BSS-vecDC provides far closer blood TAC than other competing methods. In the next section, we provide sensitivity study of this result.

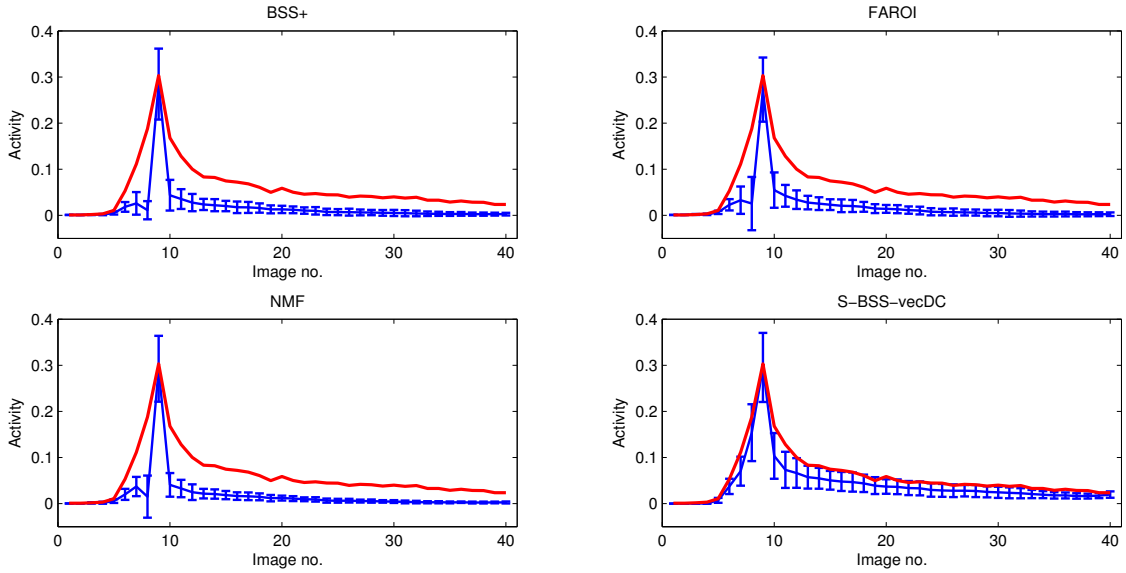

Figure 5. The calculated mean and standard deviation of blood TAC for the BSS+, FAROI, NMF, and S-BSS-vecDC algorithms are displayed. The red curve is blood TAC obtained using manually placed ROI.

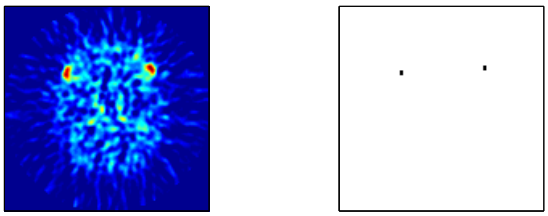

Figure 3. The source image for $n = 9$ is displayed on the left image. The manually selected ROIs of arterial veins are displayed on the right image.

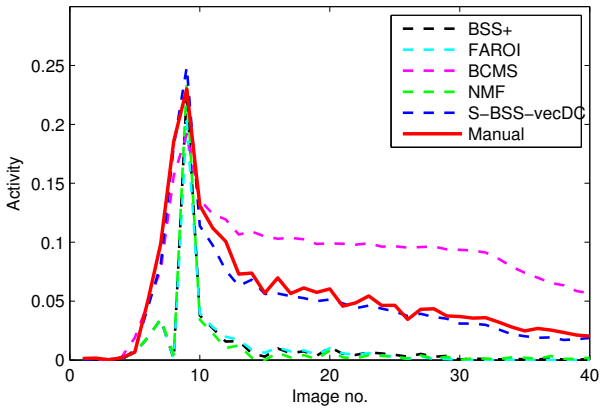

Figure 4. TACs of blood tissues from all comparing methods are shown.

A. Input Function Estimation from Slices

The goal of this experiment is to estimate input function from the whole measured volume. We will not use the BCMS algorithm in this experiment since its estimate of blood tissue is unreliable. All remaining methods are now compared.

Firstly, we created a manual ROI in several slices in the same sense as in Figure 3. We obtained a manually derived TAC of blood using this approach. Note that the blood TAC obtained manually is supposed to be slightly overestimated over the true blood curve since it contains signal from other tissues. This TAC will be used for comparison with the blood estimates from the BSS+, FAROI, NMF, and S-BSS-vecDC algorithm. Secondly, we ran the automatic algorithms on the whole volume slice by slice and the blood curves were selected for each slice. The results are displayed in Figure 5 using mean value and standard deviation at each time point. The curves are compared with manually obtained blood TAC, the red line.

The results in Figure 5 show that estimates from the S-BSS-vecDC algorithm are systematically closer to the manual method then estimates from any other algorithm. The small disproportion between manually obtained blood TAC and blood TAC from the S-BSS-vecDC algorithm is expected since manually selected ROI alway contains other tissues and therefore accumulate activity from them.

B. Input Function Estimation from the Whole Volume

The data matrix D is supposed to be $D \in \mathbf{R}^{p \times n}$ where n is the time index. In previous experiments, we ran computations for each slice, hence, our p was $128 \cdot 128$. Here, we rearrange the data matrix for the whole volume at once so that $p = 128 \cdot 128 \cdot 35$ and run the algorithms for the whole volume. We will study if the behavior of blood TACs will vary from those obtained slice by slice.

The results for blood tissue are shown in Figure 6. The BSS+ result is on the top left, the FAROI result is in the top right, the NMF result is on the bottom left, and the S-BSS-vecDC result is on the bottom right. As can be seen from the TACs, all algorithms are stable in blood TAC estimation with result from the S-BSS-vecDC algorithm being the best. How-

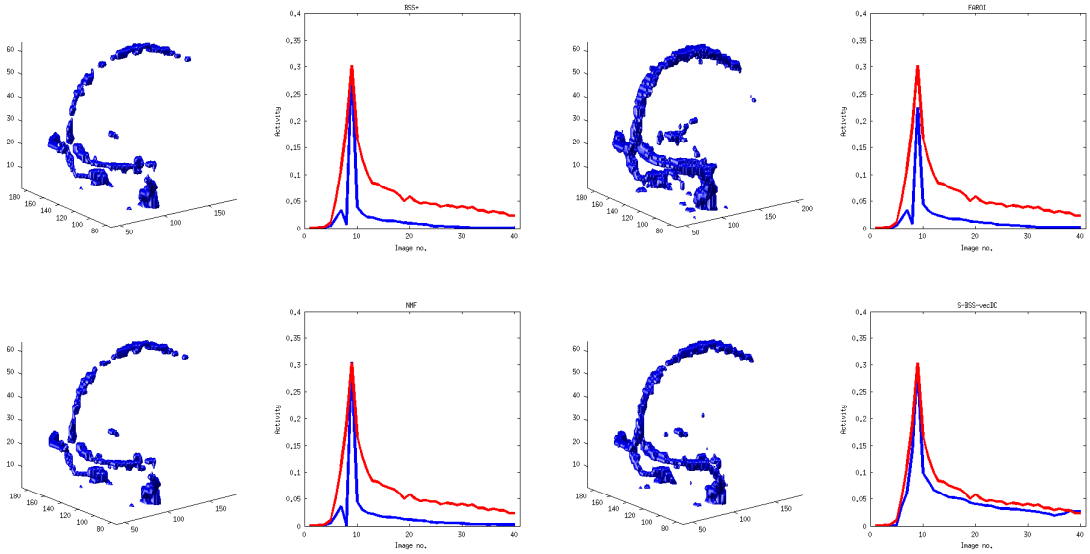

Figure 6. The blood tissues computed using the BSS+ (top left), FAROI (top right), NMF (bottom left), and S-BSS-vecDC (bottom right) algorithms from the full volume. The red curve is the blood TAC obtained using manually placed ROI.

ever, all blind source separation algorithms provide slightly lower estimates of the blood TAC than the manual method which could be caused by additional background tissue activity in manually selected blood ROI.

IV. Discussion and Conclusion

In this paper, we compare the ability of existing blind source separation algorithms to recover data from dynamic positron emission tomography where the observed images arise as a superposition of the tissue images. Specifically, we focus on clarity of separation of the blood curve which could be reliably estimated manually for this data and thus it can be used as a good reference value.

We reviewed five methods, their assumptions and underlying models. From the results of separation provided by these methods, we manually selected the sources corresponding to the blood stream and compare their TACs with the manually obtained reference. The clear winner of this comparison is the S-BSS-vecDC method [18]. Agreements of this method with manual selection is very encouraging and has the potential to replace invasive estimation of the blood curve used as the input function in various applications.

Appendix A
Truncated Normal Distribution

Truncated normal distribution, denoted as $t\mathcal{N}$, of a scalar variable x on interval $[a;b]$ is defined as

$$x \sim t\mathcal{N}(\mu,\sigma,[a,b]) = \\ = \frac{\sqrt{2}\exp((x-\mu)^2)}{\sqrt{\pi\sigma}(erf(\beta)-erf(\alpha))}\chi_{[a,b]}(x), \quad (9)$$

where $\alpha = \frac{a-\mu}{\sqrt{2\sigma}}$, $\beta = \frac{b-\mu}{\sqrt{2\sigma}}$, function $\chi_{[a,b]}(x)$ is a characteristic function of interval $[a,b]$ defined as $\chi_{[a,b]}(x) = 1$ if $x \in [a,b]$ and $\chi_{[a,b]}(x) = 0$ otherwise. $\mathrm{erf}()$ is the error function defined as $\mathrm{erf}(t) = \frac{2}{\sqrt{\pi}}\int_0^t e^{-u^2}\mathrm{d}u$. The moments of truncated normal distribution are

$$\widehat{x} = \mu - \sqrt{\sigma}\frac{\sqrt{2}[\exp(-\beta^2)-\exp(-\alpha^2)]}{\sqrt{\pi}(\mathrm{erf}(\beta)-\mathrm{erf}(\alpha))}, \quad (10)$$

$$\widehat{x^2} = \sigma + \mu\widehat{x} - \sqrt{\sigma}\frac{\sqrt{2}[b\exp(-\beta^2)-a\exp(-\alpha^2)]}{\sqrt{\pi}(\mathrm{erf}(\beta)-\mathrm{erf}(\alpha))}. \quad (11)$$

References

[1] C.M. Bishop and M.E. Tipping. Variational relevance vector machines. In *Proceedings of the 16th Conference on Uncertainty in Artificial Intelligence*, pages 46–53, 2000.

[2] B. Bodvarsson, L.K. Hansen, C. Svarer, and G. Knudsen. Nmf on positron emission tomography. In *Acoustics, Speech and Signal Processing, 2007. ICASSP 2007. IEEE International Conference on*, volume 1, pages I–309. IEEE, 2007.

[3] E. Croteau, E. Poulin, S. Tremblay, V. Dumulon-Perreault, O. Sarrhini, M. Lepage, and R. Lecomte. Arterial input function sampling without surgery in rats for positron emission tomography molecular imaging. *Nuclear medicine communications*, 35(6):666–676, 2014.

[4] R. Di Paola, J.P. Bazin, F. Aubry, A. Aurengo, F. Cavailloles, J.Y. Herry, and E. Kahn. Handling of dynamic sequences in nuclear medicine. *Nuclear Science, IEEE Transactions on*, 29(4):1310–1321, 1982.

[5] Renaud Gaujoux and Cathal Seoighe. Semi-supervised nonnegative matrix factorization for gene expression deconvolution: a case study. *Infection, Genetics and Evolution*, 12(5):913–921, 2012.

[6] G. Germano, B.C. Chen, et al. Use of the abdominal aorta for arterial input function determination in hepatic and renal pet studies. *Journal of nuclear medicine*, 33(4):613, 1992.

[7] H.N.J.M. Greuter, R. Boellaard, et al. Measurement of 18f-fdg concentrations in blood samples: comparison of direct calibration and standard solution methods. *Journal of nuclear medicine technology*, 31(4):206–209, 2003.

[8] R.N. Gunn, S.R. Gunn, and V.J. Cunningham. Positron emission tomography compartmental models. *Journal of Cerebral Blood Flow & Metabolism*, 21(6):635–652, 2001.

[9] Hyunsoo Kim and Haesun Park. Sparse non-negative matrix factorizations via alternating non-negativity-constrained least squares for microarray data analysis. *Bioinformatics*, 23(12):1495–1502, 2007.

[10] A. Kuruc, W.J.H. Caldicott, and S. Treves. Improved Deconvolution Technique for the Calculation of Renal Retention Functions. *COMP. AND BIOMED. RES.*, 15(1):46–56, 1982.

[11] D.D. Lee and H.S. Seung. Algorithms for non-negative matrix factorization. In *Advances in neural information processing systems*, pages 556–562, 2000.

[12] M. Liptrot, K.H. Adams, L. Martiny, L.H. Pinborg, M.N. Lonsdale, N.V. Olsen, S. Holm, C. Svarer, and G.M. Knudsen. Cluster analysis in kinetic modelling of the brain: a noninvasive alternative to arterial sampling. *NeuroImage*, 21(2):483–493, 2004.

[13] J.W. Miskin. *Ensemble learning for independent component analysis*. PhD thesis, University of Cambridge, 2000.

[14] C.S. Patlak, R.G. Blasberg, J.D. Fenstermacher, et al. Graphical evaluation of blood-to-brain transfer constants from multiple-time uptake data. *J Cereb Blood Flow Metab*, 3(1):1–7, 1983.

[15] D.Y. Riabkov and E.V.R. Di Bella. Estimation of kinetic parameters without input functions: analysis of three methods for multichannel blind identification. *Biomedical Engineering, IEEE Transactions on*, 49(11):1318–1327, 2002.

[16] V. Šmídl and O. Tichý. Automatic Regions of Interest in Factor Analysis for Dynamic Medical Imaging. In *2012 IEEE International Symposium on Biomedical Imaging (ISBI)*. IEEE, 2012.

[17] V. Šmídl and O. Tichý. Sparsity in Bayesian Blind Source Separation and Deconvolution. In Hendrik Blockeel et al., editor, *Machine Learning and Knowledge Discovery in Databases*, volume 8189 of *Lecture Notes in Computer Science*, pages 548–563. Springer Berlin Heidelberg, 2013.

[18] O. Tichý and V. Šmídl. Bayesian blind separation and deconvolution of dynamic image sequences using sparsity priors. *Medical Imaging, IEEE Transaction on*, 2014. (accepted, doi:10.1109/TMI.2014.2352791).

[19] O. Tichý, V. Šmídl, and M. Šámal. Model-based extraction of input and organ functions in dynamic scintigraphic imaging. *Computer Methods in Biomechanics and Biomedical Engineering: Imaging & Visualization*, 2014. (accepted, doi:10.1080/21681163.2014.916229).